Label-free RNA aptamer-based capacitive biosensor for the detection of C-reactive protein†

Anjum Qureshi, Yasar Gurbuz, Saravan Kallempudi and Javed H. Niazi*

Received 11th March 2010, Accepted 5th July 2010
DOI: 10.1039/c004133e

In this study, we report a novel aptamer-based capacitive label-free biosensor for monitoring transducing aptamer–protein recognition events, based on charge distribution under the applied frequency by non-Faradaic impedance spectroscopy (NFIS). This approach to capacitive biosensors is reported for the first time in this study, is reagent-less in processing and is developed using gold interdigitated (GID) capacitor arrays functionalized with synthetic RNA aptamers. The RNA atpamers served as biorecognition elements for C-reactive protein (CRP), a biomarker for cardiovascular disease risk (CVR). The signal is generated as a result of the change in relative capacitance occurring as a result of the formation of an RNA–CRP complex on GID capacitors with the applied AC electrical frequency (50–350 MHz). The dispersion peak of the capacitance curve was dependent on the CRP concentration and tends to shift toward lower frequencies, accompanied by the increase in relaxation time due to the increased size of the aptamer–CRP complex. The dissociation constant (K_d) calculated from the non-linear regression analysis of the relative capacitance change with the applied frequency showed that strong binding of CRP occurred at 208 MHz (K_d = 1.6 μM) followed by 150 MHz (K_d = 4.2 μM) and 306 MHz (K_d = 3.4 μM) frequencies. The dynamic detection range for CRP is determined to be within 100–500 pg ml^{-1}. Our results demonstrates the behavior of an RNA–protein complex on GID capacitors under an applied electric field, which can be extended to other pairs of affinity biomolecules as well as for the development of electrical biosensor systems for different applications, including the early diagnosis of diseases.

1. Introduction

A biosensor is a device designed to detect or quantify biomolecules and they have been widely used as a powerful analytical tool in medical diagnostics, in the food industry and in environmental, security and defence research. Biosensors can detect proteins, nucleic acids DNA sequences and can monitor antigen–antibody interactions. In principle, they are generally fabricated by immobilizing a biological receptor material on the surface of a suitable transducer that converts the biochemical signal into quantifiable electronic signals. However, there are several shortcomings as these classical biosensors composed of recognition molecules often derived of living cells, such as enzymes, receptors, and antibodies.[1–3] The main disadvantage of using antibodies is their instability due to irreversible denaturation under external environmental perturbations. Therefore, alternative routes are continuously sought after in order to develop stable biosensors with synthetic biorecognition elements.

Novel synthetic molecules such as aptamers can fill the gaps associated with biomolecules derived of living cells. Aptamers are short, single-stranded DNA or RNA oligonucleotides that can bind to their targets and offer specific properties, which favor them as new biorecognition elements for biosensors.[4] The different nature of these nucleic-acid recognition elements and their protein targets, and the unique properties of aptamers indicate great promise for designing innovative sensing protocols.[4] Most aptamer-based biosensors reported to date rely on standard sandwich-type bioaffinity assays connected to a common enzyme,[5] fluorophore,[6] or nanoparticle tracer.[7] Recently, electrochemical aptamer-based biosensors (Faradaic type) have been reported on different platforms to detect specific proteins as disease biomarkers.[5,8–10] The electrochemical-based detection process required the help of electron transfer mediators and the participation of additional substrates. In some cases, long incubation times are required due to the slow diffusion of analyte through an unstirred layer to form the immunocomplex. These disadvantages limit greatly their application in disease diagnosis.

Here, we describe a novel aptamer-based capacitive label-free biosensor for monitoring transducing aptamer–CRP recognition events based on charge distribution under the applied frequency by NFIS using capacitors made of two electrodes for ground and signal in the absence of redox mediators. NFIS is an effective method for probing biomolecular binding events such as ligand–target interactions. The measuring principle of these sensors is based on simple changes in dielectric properties, charge distribution, and conductivity changes when a ligand–target complex formed

Faculty of Engineering and Natural Sciences, Sabanci University, Orhanli, Tuzla 34956, Istanbul, Turkey.
E-mail: javed@sabanciuniv.edu; Fax: +90 (216) 483 9550; Tel: +90 (216) 483 9000 Extn. 9879

† This article was submitted as part of an issue to coincide with *Faraday Discussion* 149: Analysis for Healthcare Diagnostics and Theranostics.

on the surface of an electrode without redox mediators for non-Faradaic impedance spectroscopy.[11–14] Capacitive affinity biosensors can be constructed by immobilizing recognition elements, such as antibodies or synthetic aptamers in thin layers on the electrodes, and measuring changes in the dielectric/surface properties when an analyte binds. For providing a larger sensor surface, conductors can be made into patterns of interdigitated fingers. The capacitance between the interdigitated electrodes can then be described by the basic capacitance equation

$$C = 2n\varepsilon\varepsilon_0 A/d \quad (1)$$

where ε is the dielectric constant of the medium between the plates, ε_0 is the permittivity of free space, A is the area of the electrodes, d is the distance between the two electrodes and n is the number of electrodes. Thus, when there is a change in the dielectric properties of the material between the electrodes, a change in the capacitance will occur and it is correlated to the bound target molecules captured by the immobilized ligands on the surface. The non-specific signal can be minimized simply by washing away the unbound species on the sensor surface.[13]

There have been several reports on label-free capacitive biosensors with or without redox mediators and Faradaic or non-Faradaic techniques, respectively.[14–18] It is observed that the capacitance behavior of most sensors is often prone to large standard deviations, poor reproducibility from electrode to electrode, non-specific signals and interface behavior that is not as uniform as that of an ideal capacitor. There have been few reports in the literature that are based on non-Faradic techniques using gold interdigitated (GID) capacitors for biosensor applications for whole cells and proteins.[13,14,17,19–21] Varshney *et al.* developed a microfluidic flow cell with embedded GID array microelectrodes and integrated with magnetic nanoparticle–antibody conjugates into an impedance biosensor to rapidly detect pathogenic bacteria (*E. coli* O157 : H7).[21] In an another report, an immunosensing system was developed to detect *E. coli* and *Salmonella* based on NFIS using interdigitated electrode structures.[20] Analysis of biological cells has also been reported using interdigitated impedance sensors in microfluidic biochips.[19] Recently, an aluminium-interdigitated electrode based on NFIS has been used for the detection of immunoglobulin (IgG) and cardiac troponin T (TnT) proteins.[17] The device was able to detect TnT protein levels in human serum from patients with cardiac diseases as well as in phosphate-buffered saline in the range 0.07 to 6.83 ng ml^{-1} and 0.01 ng ml^{-1} to 5 ng ml^{-1} of TnT protein, respectively. Previously, in our laboratory, we have reported a label-free capacitive biosensor for sensitive detection of multiple biomarkers using GID capacitor arrays immobilized with pure and multiple antibodies. Here, CRP and IL6 were detected in the range 25 pg ml^{-1} to 25 ng ml^{-1} and 25 pg ml^{-1} to 1 ng ml^{-1} for TNF_α.[13]

The capacitive biosensor presented in this paper measures the capacitive term of the impedance of a GID capacitor, in the absence of redox mediators, for the detection of CRP disease markers. One of the major differences between the present study and those previously reported is the synthetic biological recognition element (RNA aptamer) that was immobilized on the GID capacitor as opposed to antibodies of animal origin. CRP is chosen as a target as it is one of the plasma proteins known as an acute-phase proteins under CVR conditions. The CVR defined by the American Heart Association (AHA) and the Center for Disease Control and Prevention (CDC) is regarded as low risk for a CRP concentration below 1.0 mg l^{-1}, moderate for 1.0 to 3.0 mg l^{-1}, and high risk for concentrations over 3.0 mg l^{-1}.[22,23] CRP can rise as high as 1000-fold because of inflammation induced by infection or injury, often leading to CVR.[24] Recent research suggests that patients with elevated basal levels of CRP are at an increased risk of diabetes and hypertension as well as cardiovascular disease.[24] Capacitive biosensors for CRP detection have been previously developed that utilized antibodies,[14] which are prone to loss of activity over a period of time. Therefore, in this study, synthetic RNA aptamers were employed as affinity ligands on GID capacitor arrays that are stable and specifically bind CRP for the development of reagent-less, label-free aptamer-based capacitive biosensors for detection of CRP.

2. Experimental

2.1 Patterning GID array electrodes for fabrication of capacitor arrays

GID array electrodes were patterned on SiO_2 surfaces using an image reversal technique. In this process, the metal layers were patterned using a dual-tone photoresist AZ5214E. A 2 μm thick AZ5214E photoresist was patterned with the help of a mask for a lift-off process in pure acetone as a solvent. Following this step, a very thin tungsten layer of 50–60 nm size was used to improve the adhesion of gold on the SiO_2 film by DC sputter deposition and about a 200–210 nm thick gold layer was deposited. The dimensions of each electrode were 800 μm in length, 40 μm in width with a distance between electrodes of 40 μm. Each capacitor sensor contained 24 interdigitated electrodes with a total area of 3 mm^2 [Fig. 1(a)]. The surface characterization was performed using atomic force microscopy (AFM, Nanoscope) in tapping mode and by optical microscopy.

2.2 Immobilization of thiolated RNA aptamer

A modified 44-mer RNA aptamer that has previously been shown to specifically bind C-reactive protein (CRP)[25] was custom synthesized after modification with an alkane thiol-linker at the 5′ end (Bioresearch Tech. Inc. USA). The resulting modified RNA aptamer had the following sequence 5′-HS-$(CH_2)_6$-GCCUGUAAGGUGGUCGGUGUGGCGA-GUGUGUUAGGAGAGAUUGC-3′. For immobilization, the capacitor arrays were first subjected to plasma cleaning and the GID region of the chips was immobilized with modified aptamer *via* self-assembled monolayer (SAM) formation by incubating 2 μl of 4, 6, and 10 μM thiol-modified RNA aptamer in phosphate-buffered saline (PBS) pH 7.2 for 2 h under sterile conditions.[26] After SAM formation, the surfaces of the capacitor chips were gently washed twice with sterile distilled water and dried over a stream of N_2 gas and stored at 4 °C until use.

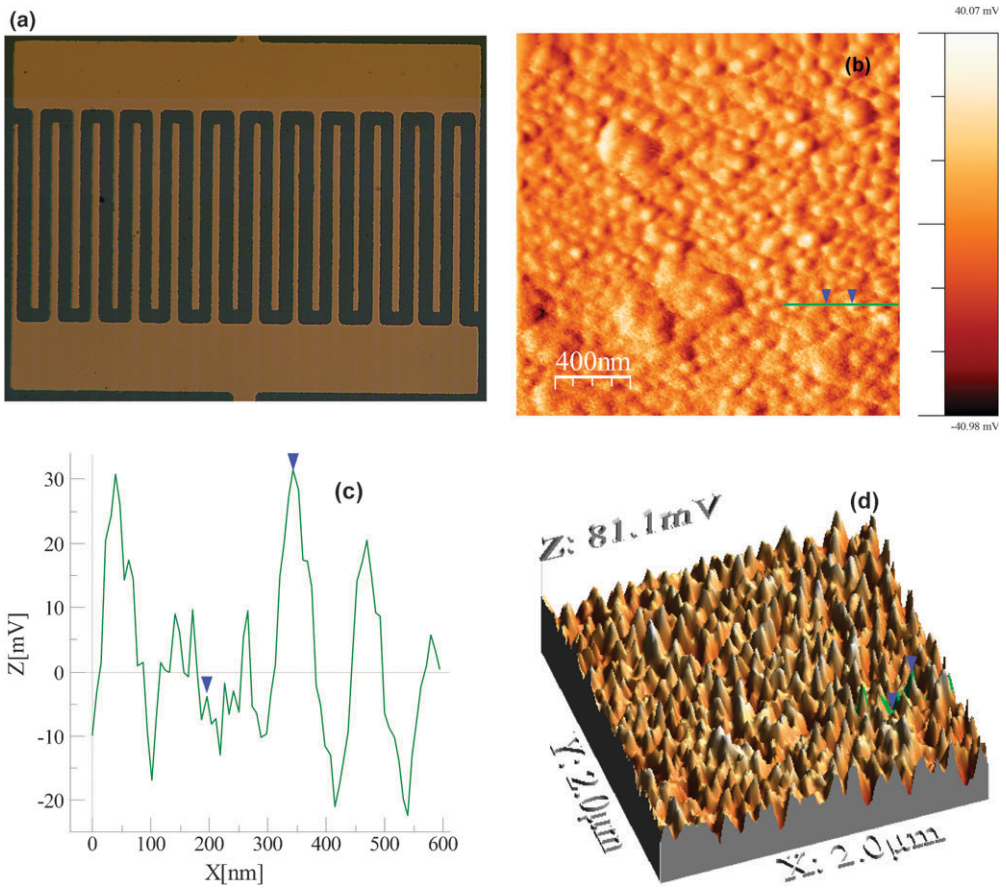

Fig. 1 (a) Optical micrograph of a GID capacitor; (b) tapping-mode AFM height image (scan area of 2 × 2 μm^2) of GID electrodes on capacitor surface; (c) Line plot surface profile of the selected green line in the AFM height image, and (d) 3D AFM topographical map of the GID electrode surface (scan area of 2 × 2 μm^2). The blue arrowheads indicate the surface topography regions of valley and height within the 120 nm green line region.

2.2 Binding assays and measurement of dielectric properties

As a prerequisite for binding assays, the immobilized aptamers were subjected to denaturation followed by renaturation in order to attain the aptamer's most stable conformation before being incubated with the target protein. This was first performed by heat denaturation of the RNA-functionalized chips at 90 °C for 5 min in a humid airtight microarray hybridization chamber after immersing it in a preheated hot water bath. This was followed by quickly cooling the chips at 4 °C for 2 min in an ice bath, and finally annealing at 25 °C for 15 min. For binding assays, the GID capacitors immobilized with different concentrations of thiol-RNA were first tested by incubating 2 μl of 100 pg ml^{-1} of CRP (Cat. No. C4063, Sigma USA). The immobilized RNA aptamer concentration that gives away a significant change in dielectric responses (impedance/capacitance) was determined, and this concentration (10 μM) was subsequently used to immobilize on all capacitor array chips for further studies.

A series of GID capacitor arrays immobilized with thiol-RNA aptamer (10 μM) were used for the binding assays against different concentrations of CRP target (0–600 pg ml^{-1}) in phosphate-buffered saline (PBS) pH 7.2. A non-specific protein, bovine serum albumin (BSA) was used as a negative control. After the capacitor chips incubated with the target molecules, these chips were then washed twice with same buffer to eliminate non-specific molecules, and dried gently under a stream of N_2 gas before they were used for dielectric measurements.

2.3 Dielectric measurements (impedance/capacitance)

The dielectric parameters were measured before and after the CRP binding on the capacitor surface by NFIS. First, the capacitance/impedance was measured sequentially after every step that includes; (a) blank-1 (bare GID capacitors), (b) after SAM formation with thiol-RNA (after immobilization, blank-2), and finally comparing the results with (e) after capturing the CRP target on the RNA-functionalized GID capacitors. The dielectric properties in between the interdigitated electrodes were measured in the frequency range 50 MHz to 1 GHz using a Network Analyzer (Karl-Suss PM-5 RF Probe Station and Agilent-8720ES). The Network Analyzer was calibrated using the SOLT (short-open-load-through) method. The impedance values were exported to Matlab for the analysis. The capacitance values were extracted at an effective frequency (f) range, and normalized with respect to blank controls. The relative capacitance variations were calculated from the data obtained within the 50–400 MHz

frequency range under standard assay conditions using eqn (2), as described previously.[17]

$$\frac{C - C_0}{C_0} \times 100 \qquad (2)$$

where C is the actual capacitance after the binding of the target CRP with RNA aptamer at a particular concentration and C_0 is the capacitance before binding. BSA protein was added in place of the CRP for determining any non-specific binding on the capacitor surface (negative control).

The time at which the polar molecule has the ability to relax under the effect of the applied field was calculated from the following equation [eqn (3)], as described previously:[27]

$$\tau = \frac{1}{2\pi f_c} \qquad (3)$$

where, f_c being the critical frequency corresponding to the maximum peak point of the dispersion curve.

2.4 Determination of dissociation constants (K_d)

In order to calculate the dissociation constants, the relative capacitance change was plotted as a function of varying CRP concentrations. The values were fitted by the non-linear regression analysis with the help of the following equation [eqn (4)] using Sigmaplot 10.0 program under ligand binding mode and the program was set with the number of binding sites equal to one.

$$y = \frac{B_{max}[\text{free CRP}]}{K_d + [\text{free CRP}]} \qquad (4)$$

where y is the degree of saturation, B_{max} is the number of maximum binding sites, and K_d is the equilibrium or dissociation constant.[28] Assuming a Langmuir adsorption isotherm, the change in relative capacitance was then directly related to the RNA aptamer binding to CRP. All experiments were performed in at least triplicate and the standard deviations are shown as errors. Inter and intra-assay relative standard deviations (RSD%) were calculated from all the experiments and were found to be within 13%.

3. Results and discussion

In this study, we report, for the first time, on the development of a label-free, reagent-less RNA aptamer-based capacitive biosensor for the detection of CRP using GID capacitor arrays. Here, the detection principle was based on the change in relative capacitance induced by the formation of a aptamer–CRP complex. Initially, the GID electrode capacitor arrays were fabricated using an image-reversal technique as described in the experimental section. The surface properties of the capacitor chips were observed by optical microcroscopy and AFM imaging [Fig. 1(a)–(d)]. An optical micrograph of the GID electrode capacitor region is shown in Fig. 1(a). The topography of the gold interdigitated electrodes on SiO_2 surface was scanned by tapping-mode AFM and showed a good distribution of the gold nanoparticles on the SiO_2 background [Fig. 1(b) and (c)]. The size of the sputtered gold nanoparticles observed was *ca.* 200–500 nm [Fig. 1(a)]. An AFM 3D height map image showed varying heights of the gold nanoparticles in a 2 × 2 μm^2 scanned area of GID electrode [Fig. 1(d)].

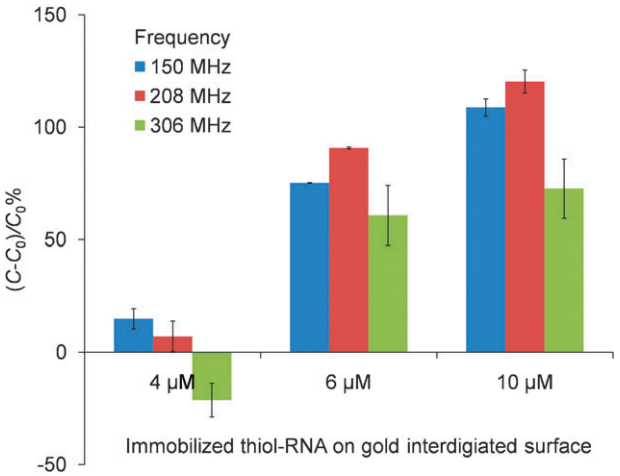

Fig. 2 Relative capacitance change occurred after immobilizing three different concentrations of thiol-modified RNA aptamer on the GID surface of the capacitors. The responses shown in the figure are derived from incubating 100 pg ml^{-1} of CRP on the aptamer-functionlized chips at three different frequencies, as indicated in the figure legend.

It was imperative to determine the density of RNA aptamers immobilized on the GID electrodes, because excessive and dense aptamers may cause steric hindrance that influences nucleic acid folding as well as the binding ability of the target molecules.[29,30] The maximum variations in relative capacitance on GID capacitor arrays was determined. It was found that 10 µM of immobilized RNA aptamer with a calculated density of 150 ng mm^{-3} gave a significant response to the tested 100 pg ml^{-1} CRP at a frequency range 50–350 MHz, with a specified GID electrode geometry as described in the experimental section and shown in Fig. 2.

3.1 Concentration-dependent response of RNA aptamer-functionalized capacitors

The concentration-dependent change in relative capacitance was tested by incubating a series of CRP concentrations (0–600 pg ml^{-1}) for 1 h on functionalized capacitor arrays (Fig. 3). A separate chip immobilized with CRP-specific RNA aptamer was incubated with a non-specific protein (BSA) that did not show any non-specific binding. It was observed that the variations in the relative capacitance responses at varying frequencies were dependent on the concentration of CRP from 100–500 pg ml^{-1} (Fig. 2 and 3). The differences and the sensitivity in response to CRP under the applied frequency could be strongly dependent on the nature of the protein as well as the specific geometry of the gold electrodes.[31,32] The response of the capacitive biosensor chip was consistent in the frequency range of 50–350 MHz for the CRP under standard assay conditions. The relative capacitance change declined with elevated CRP concentration (600 pg ml^{-1}) in the same frequency range. Under the standard conditions, the capacitive biosensor chips can bind up to a maximum of 500 pg ml^{-1} CRP concentration. The detection limit using GID capacitor chips immobilized with 10 µM of RNA aptamers was therefore determined to be within 100–500 pg ml^{-1}, which is comparable to a previous report with surface plasmon resonance (SPR) analysis.[25]

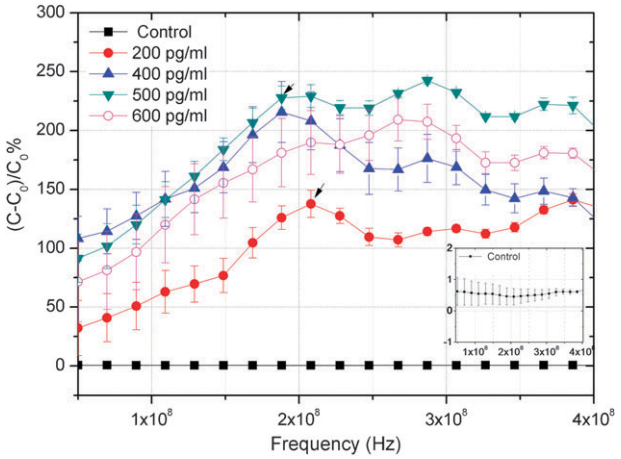

Fig. 3 Relative capacitance change (dispersion curves) obtained after the RNA aptamer-immobilized GID capacitor arrays were incubated with different concentrations of CRP. The arrows indicate the concentration-dependent shift in the peaks. The inset figure shows the relative capacitance change for the control.

3.2 Dispersion curves

It was observed that the characteristic maximum peak point of the capacitance dispersion curve tends to shift toward lower frequencies after incubating with increasing CRP concentrations (Fig. 3). This shift in dispersion curve peak can be attributed to the larger size of the aptamer–CRP complex brought on by binding with incremental CRP levels. The change in relative capacitance on the capacitor surface can occur because of the following reasons. In a complex protein, positive and negative charges come from the ionizable side chains of acidic and basic amino acids present in the protein structure, combined with negative charges on the RNA aptamer backbone. The simplest molecular dipole consists of a pair of opposite electrical charges with magnitudes of $+q$ and $-q$ and separated by r, vector distance. The molecular dipole moment m is given by the equation $m = qr$. Each type of polar or polarizable entity exhibits its own characteristic response to the imposed electric field.[33–35] When the immobilized aptamers bind their target CRP, an aptamer–CRP complex is formed. The change in conformation induced by this interaction leads to an increase in the molecular size of the aptamer–CRP complex.[36] This increase in size of the aptamer–CRP complex therefore probably leads to a relatively large permanent dipole moment.[37]

The limit of binding on the aptamer-functionalized capacitor surface was observed until all of the binding sites were occupied, which was determined to be 500 pg ml^{-1} of CRP. CRP above this level seems to create a competitive environment between the free and bound CRP molecules in order to bind RNA aptamers. This was probably because of limited binding sites on the GID surface. The competition between the free and bound CRP on the capacitor surface may have influenced the dissociation of the bound CRP over a threshold concentration ($>$500 pg ml^{-1} of CRP) that probably leads to the loss or a decline in relative capacitance change against CRP of 600 pg ml^{-1} concentration (Fig. 3).

3.3 RNA aptamer–CRP binding kinetics

Non-linear regression analysis and curve fitting of the change in relative capacitance against varying CRP concentrations applied to capacitor surfaces immobilized with RNA aptamers at a density of 150 ng mm^{-3} showed the dissociation constant, K_d was within 500 pg ml^{-1}. It was found that K_d was also affected by the applied frequency. The calculated K_d values at 150, 208 and 306 MHz frequencies were 484, 180, and 340 pg ml^{-1}, respectively with the constant RNA aptamer concentration immobilized on GID surface (Fig. 4). These results indicate that strong binding of the RNA aptamer on the capacitor surface occurred at 208 MHz compared to those found at 150 or 306 MHz frequencies.

The concentration of CRP that resulted in the maximum relative capacitance change was 500 pg ml^{-1} bound on an area of 3 mm^2 with an initial RNA aptamer density of 150 ng mm^{-3} (Fig. 3). In previous studies, a similar RNA aptamer sequence but distinctly modified at the 5′ end showed a detection range of 0.005–0.5 μg ml^{-1} with 0.1 μM of RNA aptamer immobilized on an unspecified area and measured by surface plasmon resonance (SPR) analysis.[25] However, the sensitivity was enhanced using a capacitive sensor chip and it should be noted that the concentration of RNA aptamer immobilized (10 μM) on a specified area and the geometry of the gold surface combined with denaturation and loss of RNA aptamer before the binding reaction was critical.

The kinetics of the binding reactions between RNA aptamer and CRP were further supported by the characteristic responses of the bound complex to the applied frequency and the rotational relaxation time (Table 1). The larger size/volume of the accumulating protein layer on the capacitive biosensor surface tends to possess larger relaxation times arising from the rotation of the protein molecules.[33] We observed two prominent peaks in the dispersion curves as a function of frequency with the tested CRP concentrations (Fig. 3). This could be due to the behavior of protein molecules including relaxation of proteins, and surface conduction processes associated with movements of protein bound ions

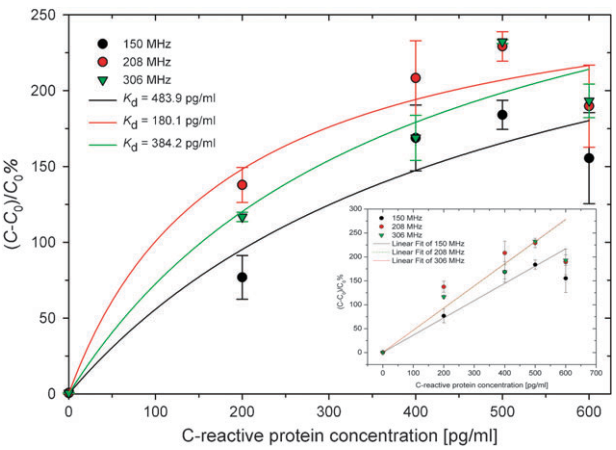

Fig. 4 Concentration-dependent change in relative capacitance occurred after RNA aptamer–CRP complex formation on GID capacitors with varying CRP concentrations at three different frequencies as shown in the legend. The inset shows the best-fit linear regression lines.

Table 1 Values of the characteristic frequency and relaxation times from capacitance dispersion peaks for different CRP concentrations

	First dispersion peak (150–250 MHz range)		Second dispersion peak (250–330 MHz range)	
CRP concentration/ pg ml^{-1}	[a]Frequency at first peak (f_1)/MHz	Relaxation time (τ_1)/ $\mu s \times 10^{-4}$	[a]Frequency at second peak (f_2)/MHz	Relaxation time (τ_2)/ $\mu s \times 10^{-4}$
200	208	7.73	300	5.31
400	194	8.21	288	5.53
500	193	8.25	286	5.57
600	—	—	273	5.83

[a] Frequency at which relative capacitance maxima was found in a dispersion curve.

under the applied electric field.[33] It was found that the two peaks of each dispersion curve shifted toward lower frequencies with higher CRP concentrations. For example, the first dispersion peak for the concentrations 200 and 500 pg ml^{-1} CRP appeared at 208 and 193 MHz frequencies, respectively. The similar shift in the dispersion curve peaks for the other concentrations often accompanied by their increased relaxation time of the RNA–CRP complex (Table 1). The shorter relaxation time with lower CRP levels can be attributed to the smaller shape/size and volume of the aptamer–CRP complex (for *e.g.*, with 200 pg ml^{-1} CRP) on GID capacitor surface. Additionally, the fact that there was no response to a non-specific protein (BSA) indicated that the sensor chips were specific to respond to CRP, an essential feature for a biosensor that finds applications in accurate diagnosis and the monitoring of disease risks.

4. Conclusion

This study demonstrates the use of synthetic biomolecules (RNA aptamers) as molecular recognition elements for capacitive, label-free, reagent-less biosensing applications that has great potential, which is an advancement in the field of biosensors to replace conventionally used antibodies often derived from animals. The RNA aptamers served as recognition elements that bind specifically to CRP, a biomarker for cardiovascular disease. The dielectric signal was generated in terms of change in relative capacitance upon molecular interaction between RNA aptamers and CRP, and formation of RNA–CRP complexes on the capacitor surface. Sensitive detection of CRP capturing by the RNA aptamer was observed in a dynamic range 100 to 500 pg ml^{-1} under standard conditions that includes the defined geometry of GID electrodes and specified biochemical assay conditions. Furthermore, this study also demonstrated the behavioral and binding kinetics of the RNA–protein interactions on the capacitive biosensor surface with respect to changing the applied frequency. The observed strong binding of RNA aptamers with CRP was also influenced by the applied frequency, because at a particular frequency (208 MHz), the binding was strong with K_d = 1.6 μM.

The presented aptamer-based, label-free capacitive biosensor chip and its features have a great potential that offers advantages of speed, simplicity, sensitivity for reagent-less and label-free detection of disease biomarkers, as well as the possibility for miniaturization for point-of-care applications, because of its compatibility with microelectronics for signal processing and storage. Furthermore, using optimized conditions, the biosensor can potentially be applied for detection of other disease markers in suspected subjects enabling early diagnosis.

Acknowledgements

We thank Bulent Koroglu for his valuable contribution to the processing of devices. We also thank the Scientific and Technological Research Council of Turkey (TUBITAK) for the financial support for this project under the contract number 107E014. The author A. Q. is also thankful for a TUBITAK Research Fellowship For Foreign Citizens (B.02.1.TBT.0.06.01-216.01-220/175).

References

1 Z. C. Sánchez-Acevedo, J. Riu and F. X. Rius, *Biosens. Bioelectron.*, 2009, **24**, 2842–2846.
2 C. Camacho, B. Chico, R. Cao, J. C. Matias, J. Hernandez, I. Palchetti, B. K. Simpson, M. Mascini and R. Villalonga, *Biosens. Bioelectron.*, 2009, **24**, 2028–2033.
3 X. Wang, M. Zhao and D. D. Nolte, *Anal. Bioanal. Chem.*, 2009, **393**, 1151–1156.
4 B. Strehlitz, N. Nikolaus and R. Stoltenburg, *Sensors (Basel, Switzerland)*, 2008, **8**, 4296–4307.
5 Y. Xu, G. F. Cheng, P. G. He and Y. Z. Fang, *Electroanalysis*, 2009, **21**, 1251–1259.
6 W. J. Wang, C. L. Chen, M. X. Qian and X. S. Zhao, *Anal. Biochem.*, 2008, **373**, 213–219.
7 T. C. Chiu and C. C. Huang, *Sensors (Basel, Switzerland)*, 2009, **9**, 10356–10388.
8 M. N. Velasco-Garcia and S. Missailidis, *Gene. Ther. Mol. Biol.*, 2009, **13**, 1–9.
9 A. Sassolas, L. J. Blum and B. D. Leca-Bouvier, *Electroanalysis*, 2009, **21**, 1237–1250.
10 L. H. Lei, Y. C. Fu, X. H. Xu, Q. J. Xie and S. Z. Yao, *Prog. Chem.*, 2009, **21**, 724–731.
11 C. Gautier, C. Esnault, C. Cougnon, J. F. Pilard, N. Casse and B. Chenais, *J. Electroanal. Chem.*, 2007, **610**, 227–233.
12 C. Tlili, H. Korri-Youssoufi, L. Ponsonnet, C. Martelet and N. J. Jaffrezic-Renault, *Talanta*, 2005, **68**, 131–137.
13 A. Qureshi, J. Niazi, S. Kallempudi and Y. Gurbuz, *Biosens. Bioelectron.*, 2010, **25**, 2318–2323.
14 A. Quershi, Y. Gurbuz, W. P. Kang and J. L. Davidson, *Biosens. Bioelectron.*, 2009, **25**, 877–882.
15 K. Zór, R. Ortiz, E. Saatci, R. Bardsley, T. Parr, E. Csoregi and M. Nistor, *Bioelectrochemistry*, 2009, **76**, 93–99.
16 S. Carrara, V. Bhalla, C. Stagni, L. Benini, A. Ferretti, F. Valle, A. Gallotta, B. Ricco and B. Samori, *Sens. Actuators, B*, 2009, **136**, 163–172.
17 E. A. de Vasconcelos, N. G. Peres, C. O. Pereira, V. L. da Silva, E. F. da Silva, Jr. and R. F. Dutra, *Biosens. Bioelectron.*, 2009, **25**, 870–876.
18 K. S. Saravan, O. Gul, H. Basaga, U. Sezerman and Y. Gurbuz, *Sens. Lett.*, 2008, **6**, 873–877.
19 P. Ertl and R. Heer, *Elektrotechnik und Informationstechnik*, 2009, **126**, 47–50.

20 O. Laczka, E. Baldrich, F. Mun oz and F. del Campo, *Anal. Chem*., 2008, **80**, 7239–7247.
21 M. Varshney, Y. Li, B. Srinivasan and S. Tung, *Sens. Actuators, B*, 2007, **128**, 99–107.
22 Y. N. Yang, H. I. Lin, J. H. Wang, S. C. Shiesh and G. B. Lee, *Biosens. Bioelectron*., 2009, **24**, 3091–3096.
23 T. A. Pearson, G. A. Mensah, R. W. Alexander, J. L. Anderson, R. O. Cannon, 3rd, M. Criqui, Y. Y. Fadl, S. P. Fortmann, Y. Hong, G. L. Myers, N. Rifai, S. C. Smith, Jr., K. Taubert, R. P. Tracy and F. Vinicor, *Circulation*, 2003, **107**, 499–511.
24 J. Casas, T. Shah, A. Hingorani, J. Danesh and M. Pepys, *J. Intern. Med*., 2008, **264**, 295.
25 A. Bini, S. Centi, S. Tombelli, M. Minunni and M. Mascini, *Anal. Bioanal. Chem*., 2008, **390**, 1077–1086.
26 M. Yang, H. Yau and H. Chan, *Langmuir*, 1998, **14**, 6121–6129.
27 K. R. Foster and H. P. Schwan, Dielectric permittivity and electrical conductivity of biological materials, in *CRC Handbook of Biological Effects of Electromagnetic Fields*, ed. C. Polk and E. Postow, 2nd edn, 1996, Boca Raton, FL, CRC Press, pp27–96.
28 M. Muller, J. E. Weigand, O. Weichenrieder and B. Suess, *Nucleic Acids Res*., 2006, **34**, 2607–2617.
29 E. J. Cho, J. R. Collett, A. E. Szafranska and A. D. Ellington, *Anal. Chim. Acta*, 2006, **564**, 82–90.
30 G. Lautner, Z. Balogh, V. Bardoczy, T. Meszaros and R. E. Gyurcsanyi, *Analyst*, 2010, **135**, 918–926.
31 A. G. Dobrikova, M. I. Dimitrov, S. G. Taneva and I. B. Petkanchin, *Colloids Surf., B*, 2007, **56**, 114–120.
32 X. Y. Song, *J. Chem. Phys*., 2002, **116**, 9359–9363.
33 R. Pethig and D. B. Kell, *Phys. Med. Biol*., 1987, **32**, 933–970.
34 R. Pethig, *Clin. Phys. Physiol. Meas*., 1987, **8**(4a), 5–12.
35 J. G. Kirkwood and J. B. Shumaker, *Proc. Natl. Acad. Sci. U. S. A*., 1952, **38**, 855–862.
36 O. Neumann, D. Zhang, F. Tam, S. Lal, P. Wittung-Stafshede and N. J. Halas, *Anal. Chem*., 2009, **81**, 10002–10006.
37 J. Antosiewicz, *Biophys. J*., 1995, **69**, 1344–1354.

